6928 *Biochemistry* **2010,** *49,* 6928–6935
DOI: 10.1021/bi100845x

BIOCHEMISTRY
including biophysical chemistry & molecular biology
Article

Toward Screening for Antibiotics with Enhanced Permeation Properties through Bacterial Porins†

Eric Hajjar,[‡] Andrey Bessonov,[∥,#] Alexander Molitor,[⊥] Amit Kumar,[‡] Kozhinjampara R. Mahendran,[∥] Mathias Winterhalter,[∥] Jean-Marie Pagès,[⊥] Paolo Ruggerone,[‡,§] and Matteo Ceccarelli*[,‡,§]

[‡]*SLACS, Istituto Officina dei Materiali del CNR, c/o Department of Physics, and* [§]*Department of Physics, University of Cagliari, I-09042 Monserrato (CA), Italy,* [∥]*School of Engineering and Science, Jacobs University, Campus Ring 1, 28759, Bremen, Germany, and* [⊥]*UMR-MD1, Faculté de Médecine, Université de la Méditerranée, IFR88, Marseille, France.* [#]*Present address: Lehrstuhl für Bioelektronik, Physik-Department, TU München, D-85748 Garching, Germany*

Received May 26, 2010; Revised Manuscript Received July 4, 2010

ABSTRACT: Gram-negative bacteria are protected by an outer membrane barrier, and to reach their periplasmic target, penicillins have to diffuse through outer membrane porins such as OmpF. Here we propose a structure−dynamics-based strategy for improving such antibiotic uptake. Using a variety of experiments (high-resolution single channel recording, Minimum Inhibitory Concentration (MIC), liposome swelling assay) and accelerated molecular simulations, we decipher the subtle balance of interactions governing ampicillin diffusion through the porin OmpF. This suggests mutagenesis of a hot spot residue of OmpF for which additional simulations reveal drastic changes in the molecular and energetic pathway of ampicillin's diffusion. Inverting the problem, we predict and describe how benzylpenicillin diffuses with a lower effective energy barrier by interacting differently with OmpF. The thorough comparison between the theoretical predictions and the three independent experiments, which were set up to measure the kinetics of transport and biological activity, gives insights on how to combine such different investigation techniques with the aim of providing complementary validation. Our study illustrates the importance of microscopic interactions at the constriction region of the biological channel to control the antibiotic flux through it. We conclude by providing a complete inventory of the channel and antibiotic hot spots and discuss the implications in terms of antibacterial screening and design.

The increasing bacterial resistance impairs the function of currently available antibiotics. Besides, we are facing a situation where there are no truly novel active antibacterial compounds in clinical trials (*1*). The reasons that have led to this alarming situation are multiple (*2*), and today, there is an urgent need for a new way to develop potent antibacterial agents while bringing them onto the market faster and at reduced costs. An emerging strategy is to pursue a rational and microscopically founded drug design that starts from the molecular knowledge of resistant mechanisms. In such bottom-up approach, structure-based and computer-assisted drug design is expected to play a central role (*3*). However, to date, most "virtual screening" strategies have traditionally focused on optimizing the association and efficiency of antibiotics for their target, overlooking all other resistance mechanisms (*3*). For instance, Gram-negative bacteria are protected by an outer membrane, and very little is known on its permeability to antibiotics, which constitute the first line of bacterial defense (*4*). Antibiotics have to diffuse passively through protein channels, known as porins, present in the Gram-negative bacterial outer membrane, and the underexpression or mutations of these porins are acknowledged mechanisms of bacterial resistance (*4*, *5*). In the case of *Escherichia coli*, the uptake of several classes of β-lactam antibiotics, a prominent group in our current antibacterial arsenal, is largely controlled by the outer membrane protein F (OmpF)[1] porin. A key feature in its structure, as seen from the X-ray structure of OmpF (*6*), is the loop L3 that folds back into the channel to form a gate, also called constriction region or eyelet region (see Supporting Information Figure S1). In addition to such spatial constriction, this region is also characterized by a strong transversal electric field, generated by negatively charged residues D113 and E117 (L3 side), that face a cluster of positively charged residues R42, R82, and R132 (anti-L3 side) (see Supporting Information Figure S1).

Several studies investigated the impact of mutations occurring at the constriction region of OmpF on the permeability of antibiotics (*7*, *8*). Interestingly, the single R132A mutation was found to dramatically increase the uptake of cefepime, a fourth generation cephalosporin β-lactam antibiotic (*8*). In a more recent study, Vidal et al. used molecular modeling to illustrate their findings that bacteria expressing the OmpF mutant D113A were more susceptible to β-lactam antibiotics (*9*). Although molecular modeling is a method of choice to rationalize the

†This study was supported by Marie Curie Research Training Network Grant MRTN-CT-2005-019335 (Translocation), Grant DFG WI-2279/18-1, the COST Action BM0701 "ATENS", the Université de la Méditerranée and Service de Santé des Armées, and by the computer center and consortiums: Cybersar, CASPUR, and CINECA through CPU-hours allocation.

*To whom correspondence should be addressed: matteo.ceccarelli@dsf.unica.it (e-mail); +390706754933 (tel); +39070510171 (fax).

[1]Abbreviations: *E. coli*, *Escherichia coli*; OmpF, outer membrane protein F; MD, molecular dynamics; SAA, solvent-accessible area; Amp, ampicillin; Benp, benzylpenicillin; Hbond, hydrogen bond; Hcontact, hydrophobic contact; rmsf, root-mean-square fluctuations; Eb, effective barrier; MIC, minimum inhibitory concentration; BLM, black lipid membrane.

 Published on Web 07/06/2010

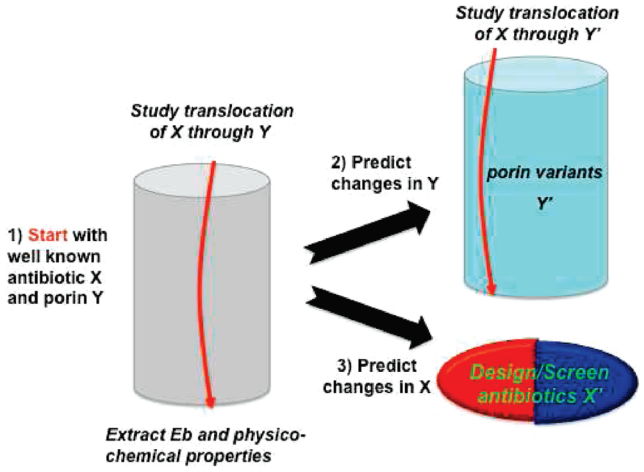

FIGURE 1: Scheme of the proposed strategy rational design/screening of antibiotic (X′) with improved permeation properties through porins (Y). The goal is to minimize the main effective barrier (Eb), and we are looking for cases where $Eb(X,Y) > Eb(X,Y') \geq Eb(X',Y)$.

antibiotic−porin interactions, the simplistic modeling protocol followed by these authors did not allow them to capture the structural and dynamic consequences of the mutation. An accurate molecular explanation appears to be necessary before any rational conclusion can be deduced from mutagenesis experiments.

In principle, standard molecular dynamics (MD) simulations would have the required microscopic accuracy to link structure and dynamics (of the drug and porin) to the rate of permeation. However, standard simulations performed in a systematic way on several porins and antibiotics would be limited to, at most, hundreds of nanoseconds and would not allow the study of the reactive pathway that antibiotics follow during passive diffusion, which is in the range of hundreds of microseconds (*10*). To overcome this time scale problem while keeping an "all atom" description of the systems, we propose to use an accelerated MD simulation algorithm scheme (*11*). We previously used the metadynamics algorithm to study the diffusion of β-lactam antibiotics through the OmpF channel (*12*), and our results suggested the important role of specific orientation and interactions of the antibiotic for the translocation process. Very recently, we have shown that kinetic properties of antibiotic diffusion can be obtained either by such high-resolution accelerated MD simulations or by single channel conductance measurements and that results from both methods agreed with spectroscopic (*13*, *14*) and flux measurements (*15*).

Supported by these agreements, we now propose to use, for the first time, an adequate in silico strategy and molecular-based approach, as schematized in Figure 1, to decipher the antibiotic−porin rate-limiting interactions with the goal of optimizing antibiotic uptake. As a starting point, we simulated and analyzed the translocation of the β-lactam ampicillin (Amp) through the porin OmpF (Figure 1, step 1). We then identified the aspartic acid residue D113 to be a hot spot and tested this hypothesis by performing an additional simulation of the translocation of Amp through the mutant OmpF-D113A (Figure 1, step 2). In the mutant porin, Amp diffuses with a lower effective energy barrier, and in-depth analysis reveals how the mutation drastically affects the physicochemical, structural, and interaction properties between drug and channel. We, then, inverted the problem (Figure 1, step 3) to predict and describe how benzylpenicillin (Bpen), by interacting differently with residue D113, translocates through OmpF with a lower effective energy barrier. Finally, to guide further studies that would aim at tuning antibiotic interactions to improve their flux, we draw, for the first time, the complete inventory of the rate-limiting interactions and map such hot spots on the structure of the OmpF porin and of the Amp and Bpen antibiotics.

To validate our computational hypothesis, we present data from three independent experimental assays that were established to measure biological activity, net flux, and kinetic properties of antibiotic permeation. To provide a clear-cut picture of such a complex and subtle process requires detailed feedback and validation procedures among different techniques. We find that each method has its own limitations and that using them independently prevents the accurate description of the complex process of antibiotic translocation. However, altogether, such a molecular-based multidisciplinary approach illustrates the importance of microscopic interactions to control the antibiotic flux through a biological channel. Our study has the potential to rationalize and accelerate the process of antibacterial research and development.

EXPERIMENTAL PROCEDURES

Molecular Simulations. The starting structure for the simulations of OmpF (crystal structure of PDB code 2OMF) and antibiotics were prepared for simulations using the program ORAC and the Amber force field, as described earlier (*12*, *16*). The process of antibiotic translocation occurs on a time scale of about 100 μs, which cannot be reached by standard MD simulations with an all-atom representation. In this study, the antibiotic translocation could be simulated thanks to the incorporation of the metadynamics simulation algorithm, which is based on a history-dependent biasing potential that discourages the system from revisiting the configurations already sampled (*11*). On the basis of previous findings (*9*, *12*, *17*), we have chosen the following collective variables for simulating antibiotic translocation using metadynamics (*11*): (i) the variable Z, defined as the difference between the coordinates of the centers of mass of the antibiotic and of the porin along the z-axis; (ii) the angle θ, defined as the orientation of the long axis of the molecule with respect to the z-axis. Due to the complexity of the process studied, we calculated the free energy after obtaining the first and only translocation path. This first crossing is considered to be the most probable path because it is passing through the lowest saddle point. We used the reconstructed free energy in the subspace of the metadynamics collective variables (*11*) to select the regions of energy minima. Additional metadynamics simulations were launched starting from each minimum, and this enabled reconstructing the one-dimensional free energy profile for the translocation of the antibiotics through OmpF-WT and the mutants. The error bars associated with the energy barrier calculations were assessed as done previously (*12*) and are of 2 kcal/mol at most. Furthermore, equilibrium MD simulations were started from each minima to analyze (using VMD (*18*) and in-house scripts) (i) the atomic root-mean-square fluctuations (rmsf), (ii) hydrogen bonds and hydrophobic interactions made by the antibiotics, and (iii) residence time of water molecules interacting with the antibiotics (*19*). Along each equilibrium simulation, we also assessed the "channel occlusion" (due to the antibiotic presence) taken as the inverse of the space available, based on calculations of the average solvent-accessible area (SAA) at cross sections corresponding to the constriction region, as done previously (*13*, *14*).

Electrophysiology Experiments. Reconstitution experiments in planar lipid bilayer and noise analysis of the ion current have been performed as described in detail previously (*10*, *17*). Lipid monolayer opposition technique was employed to form planar lipid bilayers. DPhPC was used for membrane formation. A Teflon cell with an approximately 50 μm diameter aperture in the 25 μm -thick Teflon partition and silver−silver chloride electrodes were used. Small amounts of porin (OmpF, or OmpF mutant) from a diluted stock solution of 1 mg/mL containing 1% (v/v) of octyl-POE were added to the cis side of the chamber. Spontaneous channel insertion was usually obtained while stirring under applied voltage. Conductance measurements were performed using an Axopatch 200B amplifier (Axon Instruments, Foster City, CA) in the voltage clamp mode. Signals were analyzed using a single channel analysis, as done previously (*10*, *17*, *20*). The on rate was calculated from the number of binding events ($k_{on} = v/(2[c])$, where v is number of events and [c] is the concentration of antibiotic.

The off rate ($t \gg k_{off} - 1$) was calculated from the residence time, as described previously (*10*). At the experimental conditions used here (millimolar concentration) the flux of antibiotics through the channel is proportional only to the k_{on} rate ($J = k_{on}\Delta c/2$).

Liposome Swelling Assay. Wild-type OmpF (1 mg/mL) in 1% octyl-POE was reconstituted into liposomes as described in ref *21*. *E. coli* total lipid extract (Avanti Polar lipids, Alabaster, AL) was used for liposome formation, and 17% dextran (MW 40000; Fluka) was used for the liposome filling. After incubation multilamellar liposomes were formed by sonication in a water bath sonicator. Size of formed liposomes was checked using a Nano-ZS ZEN3600 zetasizer (Malvern Instruments, U.K.). Control liposomes were prepared in the same manner without porin addition. The isotonic concentration was determined by diluting the proteoliposomes into different concentrations of raffinose (Sigma) with an Osmomat 30 osmolarimeter (Gonotec). Each batch was separated in smaller aliquots assuming a homogeneous distribution. One aliquot of each batch was tested with arabinose, a smaller molecule for which we expect maximum permeation, and this swelling rate was set at 100% for the respective batch. Normalizing each batch separately allows reducing the effects of variable reconstitution efficiencies of different preparations. Changes in optical density were monitored at 400 nm using a Cary 100 scan spectrophotometer (Varian). The swelling rates, which were averaged from at least three different sets of experiments, were calculated at pH 6 and as described by Nikaido and Rosenberg (*21*). Because of the resolution limit and large variance in these liposome-swelling assays, the measured rates only allow monitoring the presence or absence of antibiotic translocation.

Bacterial Strain, Culture Medium, and Minimun Inhibitory Concentration Assays (*MIC*). We used the same expression vector and the same host cell that we have previously described and characterized (*22*), bacteria *E. coli* BL21(DE3)Δ*omp* harboring either pColdIVompFWT or pColdIVompF113A. They were grown in Muller−Hinton (MH) broth (Difco) containing relevant antibiotic (kanamycin, 50 mg/L) (Sigma). At OD_{600} 0.4, cultures were induced with IPTG (1 mM) for 1 h at 37 °C. Bacteria were then subcultured into MH broth including IPTG and, without and with β-lactamase inhibitors (tazobactam and clavulanic acid, 4 mg/L, respectively), to quench the activity of β-lactamase expressed by *amp* gene present on plasmid (*22*). Two-fold dilution series of each antibiotic studied were prepared and added to a 1 mL aliquot of bacterial suspension in MH.

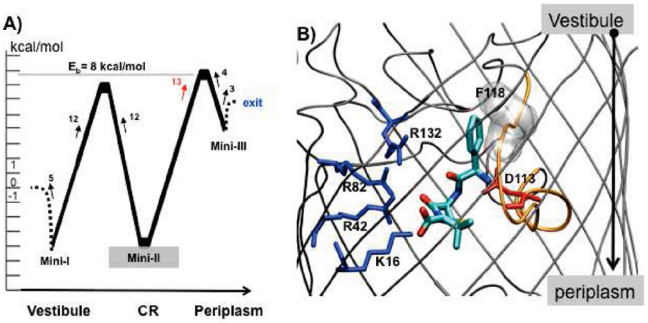

FIGURE 2: Free energy profile (A) and molecular details (B) for the diffusion of ampicilin through OmpF-WT. (A) The minimum corresponding to the affinity site at the constriction region is highlighted in gray. The energy barriers are reported in kcal/mol. (B) Snapshot at the affinity site in the constriction region (Mini-II) with the antibiotic in "sticks", colored by "atom type" (blue for nitrogen, red for oxygen, cyan for carbon), and OmpF in gray cartoons (L3 in orange). The residues making significant noncovalent, hydrogen bond and salt-bridge interactions with the antibiotic are colored by residue type (blue for positive, red for negative, green for polar), and those making hydrophobic contacts are displayed by gray molecular surface.

Assays were incubated for 18 h at 37 °C. Each assay was repeated independently four times. In order to check the correct expression of wild-type and mutated porins, SDS−PAGE and immunoblotting analyses were performed using appropriate antibodies (*22*).

RESULTS

Following the first step of our methodology (Figure 1) we find that, as Amp effectively translocates through the OmpF wild-type (WT) channel, it visits deep energy minima in three distinguishable regions: at the extracellular region (Mini-I), at the constriction region (Mini-II), and at the periplasmic region (Mini-III). To accurately quantify the diffusion process, additional metadynamics simulations were started from each identified energy minimum (see Experimental Procedures), and the calculation of free energy barriers connecting each of them allowed reconstructing the 1D free energy profile corresponding to the antibiotic diffusion (Figure 2A). The profile reveals that Amp has to overcome two large free energy barriers to translocate, a 12 kcal/mol barrier to go from Mini-I to Mini-II and a 13 kcal/mol barrier to go from Mini-II to Mini-III. We then performed in-depth qualitative analysis along the equilibrium MD simulations started from each minimum. First, we calculated the rmsf of Amp and found it to be high in all minima except in Mini-II located at the constriction zone (Table 1). This difference suggests the importance of entropy−enthalpy compensations to stabilize the Mini-II affinity site and facilitate translocation (*32*), as highlighted in a previous study in the context of biomolecular association (*23*). Indeed, such compensation is confirmed by the network of specific interactions that arise between ampicillin and OmpF in Mini-II. As highlighted in the snapshot of Figure 2B, ampicillin makes numerous noncovalent interactions and hydrogen bonds: (i) its N-terminal positive group makes a salt bridge with D113 on the L3 side, and (ii) its C-terminal negative group makes several salt bridges with R42-R82-R132 on the anti-L3 side. Furthermore, we quantified (see Experimental Procedures) the presence of "bound water molecules" based on the lifetime of their interaction with Amp (Table 1). Interestingly, only water molecules that are in fast exchange with Amp are found in Mini-I and Mini-III, as in the simulations of Amp in bulk water, unlike in Mini-II (at the constriction region) (Table 1). In Mini-II,

Table 1: Structural Details of the Antibiotic Obtained from Equilibrium MD Simulations[a]

	averaged atomic fluctuations (rmsf in Å)			interaction with "bound waters"[b]		
region of analysis	AMP-WT	AMP-D113A	Bpen-WT	AMP-WT	AMP-D113A	Bpen-WT
water box	0.99	0.99	1.15	0	0	0
Mini-I	0.74	0.42	0.83	0	6	0
Mini-II	0.29	0.82	0.48	10	0	0
Mini-III	0.40		0.72	4		0

[a] "Bound waters" were defined as the interacting molecules whose residence time is greater than 30% of the simulation time (see Experimental Procedures). [b] % of the total number of interacting water molecules is shown.

instead, water molecules are found to exchange slowly and to mediate interactions between Amp and residues at the pore walls. The conformation of Amp at the constriction region is characterized by a SAA that corresponds to the minimal area along the channel. We find that when Amp is bound in Mini-II, it occupies as much as 80% of the otherwise available space, whereas the space occupied by Amp is ~10% when Amp is in Mini-I and Mini-III.

Having identified that Mini-II is the "preferential minimum" along Amp's translocation path (highlighted in gray in Figure 2A), we can deduce that the highest energy barrier encountered from the preferential, central, minima is of 13 kcal/mol (highlighted in red in Figure 2A). While the latter value relates to the time spent by Amp in the associated affinity site (Mini-II in this case), the flux is instead defined by the value of the effective barrier (Eb), which is defined as the energy difference between the entrance of the channel and the highest barrier reached. As seen in the reconstructed 1D free energy profile (see Figure 2A), the Eb is of 8 kcal/mol in the present case.

Interestingly, we find the hydrogen bond (Hbond) between the positively charged N-terminal group of Amp and the residue D113 to be a maintained as Amp crosses the constriction region. It is only when this durable and specific interaction is disrupted that the antibiotic can cross the highest energy barrier (Figure 2A) and further diffuses down. We thus hypothesize that this salt bridge with D113 is a rate-limiting interaction that slows down the Amp translocation process. To confirm our hypothesis, we substituted the D113 amino acid by an alanine and repeated the simulation of Amp diffusion (Figure 1, step 2). Interestingly, the D113A substitution leads to important structural changes such as the enlargment of the pore (increase of 18% compared to the OmpF-WT; data not shown) and drastically affects the diffusion mechanism of Amp. We note an absence of a deep affinity site at the constriction region; instead, Amp resides just above (Mini-I) and just below (Mini-II) the constriction region. We also observe that the mutation D113A leads to the opening of a large hydrophobic pocket consituted by residues A113, M114, L115, and P116 at the constriction region. As seen in Figure 3B, as Amp reaches the constriction region, the antibiotic positions more toward the L3 loop side where its phenyl group is able to enter into the now available hydrophobic pocket. The numerous hydrophobic contacts (Figure 3B) on the N-terminal side of the antibiotic are combined to the ionic and hydrogen bond interactions on its C-terminal, whereas only hydrogen bonds are seen in the case of OmpF-WT. In the case of the OmpF mutant D113A, there is only one affinity site visited before the constriction, and we find this "preferential minima" (Mini-I) to be characterized by

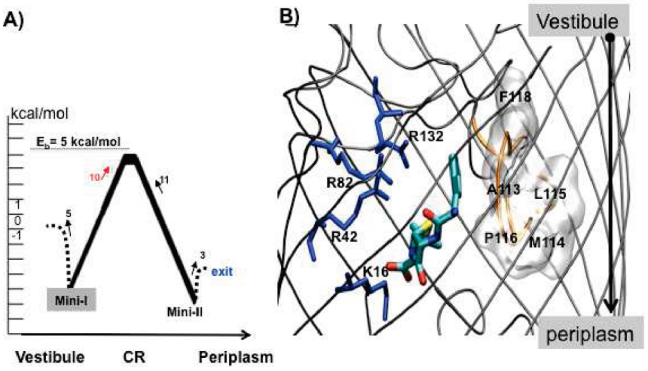

FIGURE 3: Free energy profile (A) and molecular details (B) for the diffusion of ampicilin through OmpF-D113A (see Figure 2 for legends).

(i) the smallest values of rmsf for Amp (0.42 compared to 0.82 for Mini-II), (ii) total occlusion (85% of the SAA) of the channel, and (iii) strong network of interactions of Amp with the key residues of the channel. In this case, the effective energy barrier for translocation is evaluated to be 5 kcal/mol while the highest encountered barrier, required to cross the constriction region starting from the preferential minimum (Figure 3A), is of 10 kcal/mol (both energy barriers are lower than the ones calculated in the case of the WT, Figure 2A). The different translocation mechanism translates into a different free energy profile in this case, where Amp translocates by crossing only one energy barrier, to overcome the constriction region (Figure 3A), as opposed to the two-barrier mechanism seen previously for the WT (Figure 2A). Indeed, when Amp has reached Mini-II, characterized as a transient affinity site just below the constriction region, its diffusion is then facilitated, and the barrier to exit the channel is rather small.

In order to test the theoretical predictions, we used high-resolution ion conductance measurements to experimentally access the kinetic properties of Amp translocation. The porins were reconstituted into the planar lipid bilayer, and the ion current fluctuations through single trimeric OmpF-WT or -D113A were studied in the presence of Amp. As seen from Figure 4, in the case of the OmpF-D113A mutant, the number of Amp binding events is higher compared to OmpF-WT (the number of events, calculated as explained in the Experimental Procedures section, is 120 ± 15 events/s for OmpF-D113A and 54 ± 6 events/s for OmpF-WT). The average residence time of Amp was calculated to be 170 ± 16 μs and 100 ± 10 μs in the case of OmpF-WT and OmpF-D113A channels, respectively. Thus, the results from ion conductance measurements, supporting our computational modeling, report a clear increase in the kinetics of Amp translocation for the OmpF mutant D113A and a lower residence time compared to the WT.

Altogether, our data confirm that properly optimized interactions of Amp with the channel in the constriction zone can modulate its translocation. Guided by these findings, and in particular by the determinant role of D113 seen in the mutagenesis studies, we then tackled the inverse problem (Figure 1, step 3). We predict that Bpen, whose chemical structure only differs from that of Amp by the absence of the N-terminal NH_3^+ group, would translocate with a lower energy barrier through OmpF.

Interestingly, the 1D free energy profile of the translocation of Bpen shows that we recover here the "two-barrier one binding site" scheme (Figure 5A) and that, in this case, the central minimum (Mini-II) is flanked by energy barriers that are significantly lower than for the Amp diffusion through OmpF-WT. The lower barriers can be related to an optimal interaction network of Bpen

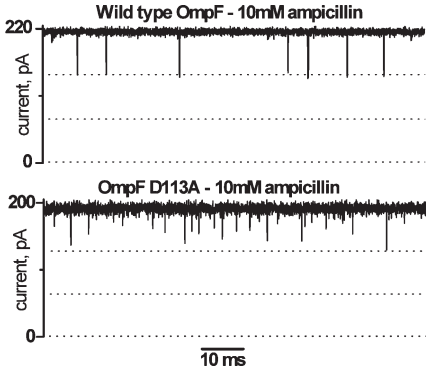

FIGURE 4: Ion current tracks through single trimeric OmpF-WT or D113A mutant reconstituted into planar lipid membranes in the presence of ampicillin and in 1 M KCl at 25 °C. Most of the time the trimeric channel is fully open. Addition of ampicillin causes temporal blocking of about one-third. The dotted horizontal lines correspond to the conductance level of one or two fully open channels.

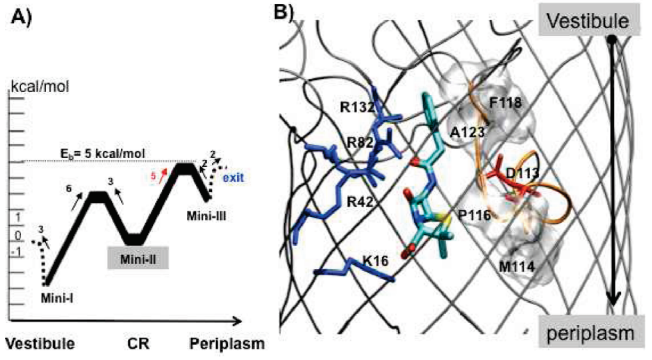

FIGURE 5: Free energy profile (A) and molecular details (B) for the diffusion of Bpen through OmpF-WT (see Figure 2 for legends).

in Mini-II where the antibiotic is localized at the constriction region and occludes 88% of the pore. As seen in Figure 5B, Bpen interacts with both the L3 and the anti-L3 sides of OmpF and with both (i) Hbonds and salt bridges via its carboxylic group and polar oxygens and (ii) hydrophobic contacts (Hcontacts) via its phenyl and dimethyl group. As expected, the Hbond between D113 and the polar nitrogen of Bpen is less durable than the corresponding one of Amp; the lifetime of this interaction is 4% of the simulation time with Bpen compared to a lifetime of 53% for the interaction between D113 and the positively charged nitrogen of Amp in the Mini-II of OmpF-WT. The lower barriers in the case of Bpen can also be related to the different solvation and flexibility patterns, as we note an absence of bound water molecules and an increased flexibility of Bpen in Mini-II compared to Amp (Table 1).

The simulations predict that the diffusion of Bpen through OmpF-WT requires a low effective barrier of 5 kcal/mol. Interestingly, the latter Eb value is identical to the one of the highest energy barrier needed to cross the identified preferential minima Mini-II (Figure 2A).

To conclude, we find the effective barrier of Bpen in OmpF-WT to be lower than the one of Amp in OmpF-D113A (Figure 3A) and Amp in OmpF-WT (Figure 2A).

Ion conductance measurements at different temperatures were then performed using the BLM technique to assess the interaction of Bpen with OmpF reconstituted in a phospholipid bilayer. As seen in Figure 6A, at room temperature the presence of 10 mM Bpen caused no significant blockage of ionic current through a single trimeric OmpF channel revealing negligible interaction

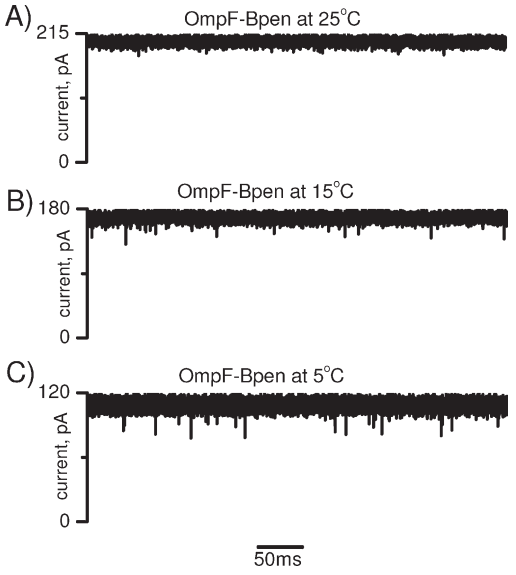

FIGURE 6: Typical ion current tracks through OmpF-WT in the presence of 10 mM Bpen measured at 25 °C (A), 15 °C (B), and 5 °C (C). Conditions: 1 M KCl, pH 6, and applied voltage 50 mV.

with the channel. We then lowered the temperature to slow the kinetics, which may increase the resolution at which ion current blockages by antibiotic can be seen. Interestingly, at low temperature (5 °C), Bpen showed very short and partial ion current flickerings (Figure 6C). However, unlike Amp, which blocks complete monomer of a single OmpF trimer (Figure 4), in the case of Bpen, blockage events are not well-defined. The fact that we are not able to resolve binding events with the BLM technique and that quantitative analysis is not possible in this case can be due to the fact either (i) that Bpen translocates through OmpF too fast to be resolved or (ii) that Bpen does not translocate at all through the OmpF channel.

In order to rule out one of the above hypotheses, we probed the net flux of Amp and Bpen through OmpF channels by applying a second experimental technique, called liposome swelling assay (*24*). Upon reconstitution of wild-type OmpF into the liposomes, we measured the permeability using arabinose as a control, as done previously (*21*, *24*), and obtained results proving that both Amp and Bpen permeate through OmpF (see Supporting Information Figure S2). The limited resolution and sensitivity of the liposome swelling method, in particular when comparing fluxes of differently charged solutes (*21*), do not allow to clearly discriminate between the two antibiotic fluxes. Clearly, the net flux measured by liposome swelling supports the first hypothesis; that is, the lack of resolved events from electrophysiology is related to a faster translocation of Bpen compared to Amp through OmpF-WT. It is worthwhile to point out that these findings illustrate the necessity of complementing different techniques to get the reliable picture, at a molecular level, of such a complex and delicate process, as antibiotic permeation through bacterial porins.

Taking advantage of the microscopic details that molecular simulations provide, we conclude, by drawing in Figure 7, the complete inventory of the identified key interactions, mapped on both antibiotic and porin structures.

Panels A and B of Figure 7 highlight the most conserved interactions for each antibiotic functional group. For example, the strongly conserved salt bridge between the antibiotic carboxylic group and either of R132, R82, R42, or K16 located at

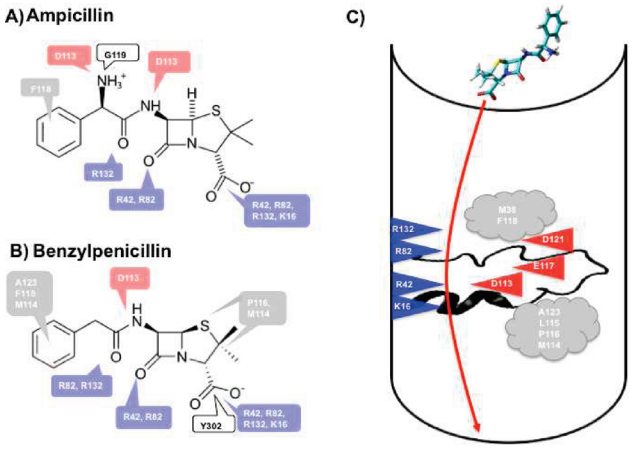

FIGURE 7: Key interactions mapped on the functional groups of (A) Amp and (B) Bpen and (C) on a scheme representing OmpF (loop L3 defining the constriction region is colored in black). We considered the most significant interactions from the equilibrium MD simulations at the affinity site of the constriction region. The hydrogen bonds and salt bridges are highlighted in boxes (A and B) or by a triangle (C) colored by residue type (blue for positive, red for negative, black for neutral amino acids), and hydrophobic contacts are in gray shading (A−C).

the anti-L3 side is expected to be a key determinant to facilitate the antibiotic diffusion as it properly orients the compounds with their C-terminal pointing down. According to our results, Bpen makes more hydrophobic contacts than Amp; in particular, its dimethyl and phenyl groups match well with the two hydrophobic pockets, composed of residues M38, M114, L115, P116, and F118, and located at the L3 side of the constriction region. Finally, Figure 7C sums up the diverse key residues that both antibiotics have to deal with as they cross the constriction region, highlighting the inner complexity of the channel and revealing the localization of well-defined hydrophobic pockets above and below the constriction region, the basic clusters on the anti-L3 side, and the acidic residues, of which D113 is seen to be the most central and exposed residue.

Biological Activity. Further, we performed some bacterial killing assays to assess the biological activity of the penicillin class and the role of the residue D113.

Due to the expression of β-lactamase in the strain, it is not possible to quantify directly the absolute impact of the mutation. However, we can conclude in an indirect manner on the relative effect of the mutation for each antibiotic. As done previously (*22*), we expressed OmpF channels as the sole porin in the outer membrane of a porin-null *E. coli* strain and used MIC assays to determine the ability of both Amp and Bpen to traverse the outer membrane via OmpF channels and kill bacteria. The same porin-deleted strain was used to express both the normal WT OmpF (D113) or mutated OmpF-D113A, which allowed comparing the role of residue D113A in the antibiotic susceptibility. Amp and Bpen belong to the same β-lactam subgroup (*25*) and have similar target; thus by measuring the level of MIC reduction toward the two β-lactams in wild-type OmpF and 113A producing bacteria while using the same host cell, we directly focus our measurements on the drug uptake.

From our results (reported in Table 2) it is quite clear that the substitution D113A increases the susceptibility for both Amp and Bpen. As seen in Table 2, the effect of the mutation on Bpen influx, where the MIC value is reduced by a factor 4 as it goes from 256 mg/L for WT to 64 mg/L for D113A, is less marked compared to the corresponding one on Amp influx, for which the MIC value is reduced by a factor of 16 as it goes from 16 mg/L for WT to 1 mg/L for D113A. Such a drastic reduction of the MIC value in the case of Amp suggests that Bpen is less dependent on an interaction with D113 during its translocation through OmpF, compared to Amp. This finding is in agreement with the computational results.

Table 2: Penicillin Susceptibility for OmpF-WT and D113A Mutant[a]

	MIC (mg/L)	
penicillin	OmpF-WT	mutant (D113A)
penicillin A group		
ampicillin	> 512	> 512
ampicillin + inhibitors	16	1
penicillin G group		
benzylpenicillin	> 512	> 512
benzylpenicillin + inhibitors	256	64

[a]Inhibitors comprise tazobactam and clavulanic acid.

DISCUSSION

Here we used all-atom molecular simulations to follow the paradigm for selecting antibiotics with better permeation properties. This has only recently been made possible by the development of accurate accelerated algorithm (*11*) and computer power. The high resolution in time and space that metadynamics simulations provide was used to characterize the molecular basis of translocation of antibiotics through OmpF-WT and its D113A mutant. However, to treat patients, it is not possible to modify the porins of bacteria, and in this study, we propose a methodology to invert the problem (Figure 1). Starting from the extensive study of a model antibiotic (X) interacting with a WT porin (Y), and using mutagenesis on the porin (Y′) as a tool, the goal is to help predict modifications of a given antibiotic (X′) so that it penetrates with a higher flux through the WT porin of interest (Y).

We further made a point of supporting this proof of concept by preparing three independent experimental setups. First, conductance measurements report a clear increase in the kinetics of Amp translocation and a lower residence time when changing from OmpF-WT to the mutant D113A. On the other hand, in the case of Bpen, only short flickering was observed, and the binding kinetics of translocation could not be obtained from the measurements. The energy barriers extracted from the MD simulations allow rationalizing both the increase of events in the case of the mutant D113A and the lack of resolved events in the case of Bpen. Indeed, we find the highest energy barrier (that informs on antibiotic residence time in the associated preferential minima) to be even lower for Bpen (5 kcal/mol) than the one of Amp through OmpF-D113A (10 kcal/mol), which was already lower than Amp through OmpF-WT (13 kcal/mol). Furthermore, for Amp through OmpF-D113A the measured residence time being 100 μs, it is at the lower limit of the electrophysiology method resolution (*26*). The fact that Bpen does indeed translocate through OmpF was further validated by the liposome swelling assays that measured its positive net flux through OmpF. Thus we hypothesize that, in the case of Bpen, the absence of ionic current blockages at room temperature as well as the very short ion current flickering is due to the very low residence time of Bpen in Mini-II. Finally, biological assays measuring antibiotic susceptibilities also showed in vivo that the uptake rate of Amp

was much more affected by the mutation of the residue D113 compared to Bpen.

Altogether, our study supports the idea that a subtle balance of interactions, localized mainly at the channel constriction region, governs the diffusion of the antibiotic through OmpF. We find this to be valid, both (i) when mutating the channel and (ii) by modifying chemically the antibiotic. We indeed identified the interaction with the residue D113 as rate-limiting, which is in agreement with the study of Vidal et al. (*9*), who described it as the "most likely interacting residue". In fact, this residue sits in the middle of both a polar and a hydrophobic cluster. Interestingly, only Bpen and not Amp is able to exploit both polar and hydrophobic interactions, and this can be related to the differences in the surface properties of the antibiotics (*27*). Indeed, we find that, although Amp has a slightly bigger molecular surface size than Bpen (305 Å^2 compared to 265 Å^2), the main difference is that Amp is found to be much more polar (its polar surface represents 73% of the total surface compared to 53% for Bpen) while Bpen is much more hydrophobic (its hydrophobic surface represents 47% of the total surface compared to 17% for Amp).

In the case of Bpen, hydrophobic interactions play an important contribution and could be an additional driving force for optimal translocation. Such a possible contribution from hydrophobicity has already been raised in the pioneer work of Nikaido (*24*). Interestingly, when D113 is mutated to an alanine, a large hydrophobic pocket opens, which perturbs the otherwise present electrostatic field, and there is a disruption of the affinity site for Amp at the constriction region. This drastic structural effect induced by the mutation suggests using caution when extrapolating the effects of experimental mutations, as it has been done often in the past, without support from techniques giving microscopic resolution and providing insights into the molecular mechanisms. Molecular simulations can, in contrast, give an accurate description of the changes induced by mutations on the transport properties, and such structural/dynamical information should be taken into account to complement and, especially, to rationalize experimental findings (*7*−*9*).

It is of interest to mention that the D113 residue, on the L3 side, participates actively to the screening of certain charged molecules translocating through OmpF. On the anti-L3 side, we note the presence of the basic residues oriented as a staircase (R167, R168, K80, R132, R82, R42, K16, respectively, from vestibule to periplasmic) along one side of the channel (see Figure 7), which is in agreement with a similar arginine ladder that was shown to facilitate phosphate transfer in the OM protein OprP (*28*, *29*). Such key structural properties contribute to the efficiency of the permeability barrier as the first defense line against toxic compounds (*30*). Consequently, another outcome of our study is that the identified "hot spots", both on the antibiotics (Figure 7A,B) and on the porin (Figure 7C) side, could be integrated in a pharmacophore model and used for in silico screening. The strategy of "using old drugs for new uses", by integrating the requirements for optimal translocation with an efficient screening of existing drugs, might lead to the discovery of better drugs at a reduced cost (*3*, *31*). Our approach also opens the way to rational chemical modifications of antibiotics with the goal of improving uptake through bacterial porins. Keeping in mind that the design of potent antibiotics is a rather complex problem, we propose that our approach could be efficiently used in conjunction with strategies tackling other effects/mechanisms to better circumvent and combat bacterial resistance(*3*). Finally, we expect that our methodology can be conveniently employed to study further porin−antibiotic interactions in other enterobacterial pathogens of interest (*4*, *5*).

ACKNOWLEDGMENT

We thank Chloe E. James for donating BL21(DE3)omp8 and OmpF plasmids. We acknowledge Jean-Michel Bolla, Anne Davin, Jurg Dreier, and Malcom Page for helpful discussions.

SUPPORTING INFORMATION AVAILABLE

Two animated videos which are the result of the translocation simulations of (1) Amp through OmpF-WT and (2) Bpen through OmpF-WT (the coloring code employed is the same as in Figure 2B) and two figures highlighting the constriction region on the structure of OmpF (Figure S1) and the liposome swelling assays results (Figure S2). This material is available free of charge via the Internet at http://pubs.acs.org.

REFERENCES

1. Arias, C. A., and Murray, B. E. (2009) Antibiotic-resistant bugs in the 21st century—a clinical super-challenge. *N. Engl. J. Med. 360*, 439–443.
2. Fischbach, M. A., and Walsh, C. T. (2009) Antibiotics for emerging pathogens. *Science 325*, 1089–1093.
3. Barker, J. (2006) Antibacterial drug discovery and structure-based design. *Drug Discovery Today 11*, 391–404.
4. Nikaido, H. (2003) Molecular basis of bacterial outer membrane permeability revisited. *Microbiol. Mol. Biol. Rev. 67*, 593–656.
5. Pages, J. M., James, C. E., and Winterhalter, M. (2008) The porin and the permeating antibiotic: a selective diffusion barrier in Gram-negative bacteria. *Nat. Rev. Microbiol. 6*, 893–903.
6. Cowan, S. W., Schirmer, T., Rummel, G., Steiert, M., Ghosh, R., Pauptit, R. A., Jansonius, J. N., and Rosenbusch, J. P. (1992) Crystal structures explain functional properties of two *E. coli* porins. *Nature 358*, 727–733.
7. Jeanteur, D., Schirmer, T., Fourel, D., Simonet, V., Rummel, G., Widmer, C., Rosenbusch, J. P., Pattus, F., and Pages, J. M. (1994) *Proc. Natl. Acad. Sci. U.S.A. 91*, 10675–10679.
8. Bredin, J., Saint, N., Mallea, M., De, E., Molle, G., Pages, J. M., and Simonet, V. (2002) Alteration of pore properties of *Escherichia coli* OmpF induced by mutation of key residues in anti-loop 3 region. *Biochem. J. 363*, 521–528.
9. Vidal, S., Bredin, J., Pages, J. M., and Barbe, J. (2005) Beta-lactam screening by specific residues of the OmpF eyelet. *J. Med. Chem. 48*, 1395–1400.
10. Nestorovich, E. M., Danelon, C., Winterhalter, M., and Bezrukov., S. M. (2002) Designed to penetrate: time-resolved interaction of single antibiotic molecules with bacterial pores. *Proc. Natl. Acad. Sci. U.S.A. 99*, 9789–9794.
11. Laio, A., and Parrinello, M. (2002) Escaping free-energy minima. *Proc. Natl. Acad. Sci. U.S.A. 99*, 12562–12566.
12. Ceccarelli, M., Danelon, C., Laio, A., and Parrinello, M. (2004) Microscopic mechanism of antibiotics translocation through a porin. *Biophys. J. 87*, 58–64.
13. Mach, T., Neves, P., Spiga, E., Weingart, H., Winterhalter, M., Ruggerone, P., Ceccarelli, M., and Gameiro, P. (2008) Facilitated permeation of antibiotics across membrane channels—interaction of the quinolone moxifloxacin with the OmpF channel. *J. Am. Chem. Soc. 130*, 13301–13309.
14. Mahendran, K. R., Hajjar, E., Mach, T., Lovelle, M., Kumar, A., Sousa, I., Spiga, E., Weingart, H., Gameiro, P., Winterhalter, M., and Ceccarelli, M. (2010) Molecular basis of enrofloxacin translocation through OmpF, an outer membrane channel of *Escherichia coli*—when binding does not imply translocation. *J. Phys. Chem. B 114*, 5170–5179.
15. Hajjar, E., Mahendran, K. R., Kumar, A., Bessonov, A., Petrescu, M., Weingart, H., Ruggerone, P., Winterhalter, M., and Ceccarelli, M. (2010) Bridging timescales and length scales: from macroscopic flux to the molecular mechanism of antibiotic diffusion through porins. *Biophys. J. 98*, 569–575.
16. Hajjar, E., Kumar, A., Ruggerone, P., Ceccarelli, M. (2010) Investigating reaction pathways in rare events simulations of antibiotics

diffusion through protein channels, *J. Mol. Model.* (DOI 10.1007/s00894-010-0698-4).
17. Danelon, C., Nestorovich, E. M., Winterhalter, M., Ceccarelli, M., and Bezrukov, S. M. (2006) Interaction of zwitterionic penicillins with the OmpF channel facilitates their translocation. *Biophys. J. 90*, 1617–1627.
18. Humphrey, W., Dalke, A., and Schulten, K. (1996) VMD: visual molecular dynamics. *J. Mol. Graphics 14* (33−38), 27–38.
19. Sterpone, F., Ceccarelli, M., and Marchi, M. (2001) Dynamics of hydration in hen egg white lysozyme. *J. Mol. Biol. 311*, 409–419.
20. Weingart, H., Petrescu, M., and Winterhalter, M. (2008) Biophysical characterization of in- and efflux in Gram-negative bacteria. *Curr. Drug Targets 9*, 789–796.
21. Nikaido, H., and Rosenberg, E. Y. (1983) Porin channels in *Escherichia coli*: studies with liposomes reconstituted from purified proteins. *J. Bacteriol. 153*, 241.
22. James, C. E., Mahendran, K. R., Molitor, A., Bolla, J. M., Bessonov, A. N., Winterhalter, M., and Pages, J. M. (2009) How beta-lactam antibiotics enter bacteria: a dialogue with the porins. *PLoS One 4*, e5453.
23. Dunitz, J. D. (1995) Win some, lose some: enthalpy-entropy compensation in weak intermolecular interactions. *Chem. Biol. 2*, 709–712.
24. Yoshimura, F., and Nikaido, H. (1985) Diffusion of beta-lactam antibiotics through the porin channels of *Escherichia coli* K-12. *Antimicrob. Agents Chemother. 27*, 84–92.
25. Bryskier, A. (2005) Antimicrobial Agents: Antibacterials and Antifungals.
26. Kozhinjampara, M., Chimerel, C., Mach, T., and Winterhalter, M. (2009) Antibiotic translocation through membrane channels: temperature-dependent ion current fluctuation for catching the fast events. *Eur. Biophys. J. 38*, 1141–1145.
27. Pyrkov, T. V., Chugunov, A. O., Krylov, N. A., Nolde, D. E., and Efremov, R. G. (2009) PLATINUM: a web tool for analysis of hydrophobic/hydrophilic organization of biomolecular complexes. *Bioinformatics 25*, 1201–1202.
28. Moraes, T. F., Bains, M., Hancock, R. E., and Strynadka, N. C. (2007) An arginine ladder in OprP mediates phosphate-specific transfer across the outer membrane. *Nat. Struct. Mol. Biol. 14*, 85–87.
29. Pongprayoon, P., Beckstein, O., Wee, C. L., and Sansom, M. S. (2009) Simulations of anion transport through OprP reveal the molecular basis for high affinity and selectivity for phosphate. *Proc. Natl. Acad. Sci. U.S.A. 106*, 21614–21618.
30. Davin-Regli, A., Bolla, J. M., James, C. E., Lavigne, J. P., Chevalier, J., Garnotel, E., Molitor, A., and Pages, J. M. (2008) Membrane permeability and regulation of drug "influx and efflux" in enterobacterial pathogens. *Curr. Drug Targets 9*, 750–759.
31. Chong, C. R., and Sullivan, D. J., Jr. (2007) New uses for old drugs. *Nature 448*, 645–646.
32. Kumar, A.; Hajjar, E.; Ruggerone, P., and Ceccarelli, M. (2010) Molecular simulations reveal the mechanism and the determinants for ampicillin translocation through OmpF. *J. Phys. Chem. B*, in press.